

Creating Impactful Characters: Correcting Human Impact Accelerations using High Rate IMUs in Dynamic Activities

CALVIN KUO, University of British Columbia, Canada

ZIHENG LIANG, University of British Columbia, Canada

YE FAN, University of British Columbia, Canada and Vital Mechanics Research, Canada

JEAN-SÉBASTIEN BLOUIN, University of British Columbia, Canada

DINESH K. PAI, University of British Columbia, Canada and Vital Mechanics Research, Canada

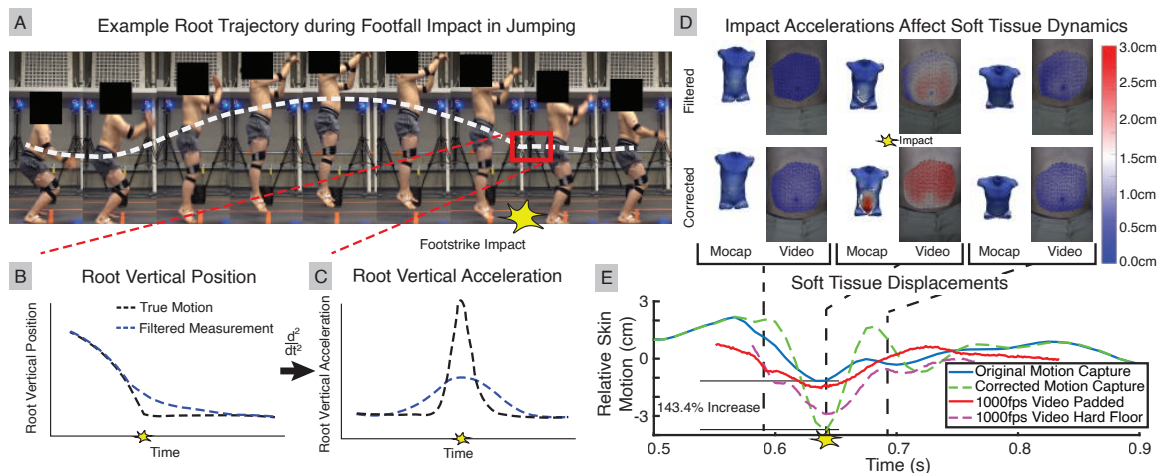


Fig. 1. Correcting impact accelerations for impactful characters: Motion capture of dynamic activities such as (A) jumping estimate generalized coordinates such as the (B) pelvis vertical position well, but can filter (C) accelerations at the impact. (D) Correcting the impact acceleration magnitude with a sparse set of higher rate IMUs can produce more dynamic soft tissue animations, as soft tissue motion is excited by body accelerations. (E) Corrections to jumping impacts produced a 143.4% increase in soft tissue motion at the stomach for a generic male with an increase in impact acceleration of 73.6%. Similar increases in soft tissue motion from filtered motion capture to corrected accelerations is observed using high speed video of a subject jumping on a soft pad to represent the effect of low-pass filters in motion capture, and on a hard surface to represent corrected ground-truth accelerations.

Human motion capture using video-based or sensor-based methods gives animators the capability to directly translate complex human motions to create lifelike character animations. Advances in motion capture algorithms have improved their accuracy for estimating human generalized motion coordinates (joint angles and body positions). However, the traditional motion capture pipeline is not well suited to measure short duration, high acceleration impacts, such as running and jumping footstrikes. While high

acceleration impacts have minimal influence on generalized coordinates, they play a big role in exciting soft tissue dynamics.

Here we present a method for correcting motion capture trajectories using a sparse set of inertial measurement units (IMUs) collecting at high sampling rates to produce more accurate impact accelerations without sacrificing accuracy of the generalized coordinates representing gross motions. We demonstrate the efficacy of our method by correcting human motion captured experimentally using commercial motion capture systems with high rate IMUs sampling at 400Hz during basketball jump shots and running. With our method, we automatically corrected 185 jumping impacts and 1266 running impacts from 5 subjects. Post correction, we found an average increase of 84.6% and 91.1% in pelvis vertical acceleration and ankle dorsiflexion velocity respectively for basketball jump shots, and an average increase of 110% and 237% in pelvis vertical acceleration and ankle plantarflexion velocity respectively for running. In both activities, pelvis vertical position and ankle angle had small corrections on average below 2.0cm and 0.20rad respectively. Finally, when driving a human rig with soft tissue dynamics using corrected motions, we found a 143.4% and 11.2% increase in soft tissue oscillation amplitudes in basketball jump shots and running respectively. Our methodology can be generalized to correct impact accelerations for other body segments, and provide new tools to create realistic soft tissue animations during dynamic activities for more lifelike characters and better motion reconstruction for biomechanical analyses.

Authors' addresses: Calvin Kuo, University of British Columbia, Vancouver, BC, Canada, calvin.kuo@ubc.ca; Ziheng Liang, University of British Columbia, Vancouver, BC, Canada, zhliang@cs.ubc.ca; Ye Fan, University of British Columbia, Vancouver, BC, Canada , Vital Mechanics Research, Vancouver, BC, Canada, yefan@cs.ubc.ca; Jean-Sébastien Blouin, University of British Columbia, Vancouver, BC, Canada, jean-sebastien.blouin@ubc.ca@ubc.ca; Dinesh K. Pai, University of British Columbia, Vancouver, BC, Canada , Vital Mechanics Research, Vancouver, Canada, pai@cs.ubc.ca.

Permission to make digital or hard copies of all or part of this work for personal or classroom use is granted without fee provided that copies are not made or distributed for profit or commercial advantage and that copies bear this notice and the full citation on the first page. Copyrights for components of this work owned by others than the author(s) must be honored. Abstracting with credit is permitted. To copy otherwise, or republish, to post on servers or to redistribute to lists, requires prior specific permission and/or a fee. Request permissions from permissions@acm.org.

© 2019 Copyright held by the owner/author(s). Publication rights licensed to ACM. 0730-0301/2019/7-ART47 \$15.00
<https://doi.org/10.1145/3306346.3322978>

CCS Concepts: • Computing methodologies → Motion capture; Physical simulation.

Additional Key Words and Phrases: Motion capture, inertial measurement units, soft tissue dynamics, impacts

ACM Reference Format:

Calvin Kuo, Ziheng Liang, Ye Fan, Jean-Sébastien Blouin, and Dinesh K. Pai. 2019. Creating Impactful Characters: Correcting Human Impact Accelerations using High Rate IMUs in Dynamic Activities. *ACM Trans. Graph.* 38, 4, Article 47 (July 2019), 12 pages. <https://doi.org/10.1145/3306346.3322978>

1 INTRODUCTION

Video-based motion capture systems such as VICON (Oxford Metrics, UK) are ubiquitous in computer animation for driving life-like character animations using real human motion [Gleicher 1999; Pullen and Bregler 2002]. While video-based systems are considered the gold standard, high quality systems require careful calibration and are restricted to specialized motion capture studios due to the large amount of equipment [Moeslund and Granum 2001; Moeslund et al. 2006]. More recent work has introduced algorithms to extract human motion from standard video cameras such as those found in smart phones [Cao et al. 2017; Ionescu et al. 2014; Kanazawa et al. 2018; Wei et al. 2016]. However, these systems are limited by camera hardware, which typically have low sampling rates, and the inherent process of extracting 3D poses from 2D images.

Over the last two decades, inertial measurement units (IMUs) utilizing a triaxial accelerometer, triaxial gyroscope, and commonly a triaxial magnetometer have been finding greater use as they allow animators to capture motion in most environments without being restricted by video equipment [Roetenberg et al. 2009; Seel et al. 2014; Vlasic et al. 2007]. Together, these systems are providing animators with powerful tools to easily create impactful character animations.

While both video-based and sensor-based motion capture methods can provide accurate estimates of generalized coordinates (joint angles and body positions), they often suffer in measuring generalized velocities and accelerations [Cerveri et al. 2003, 2005; Miranda et al. 2013a,b]. This is because motion signals are typically filtered below 20Hz to remove sources of sensor noise (such as skin motion artifacts) [Bates et al. 2013; Clark et al. 2012; Ford et al. 2000; Giakas and Baltzopoulos 1997; Hamner et al. 2010; Riemer et al. 2008; Winby et al. 2009]. While filtering in this manner is usually sufficient, it can remove true motion signals during dynamic activities. In particular, it is known that short duration, high acceleration impact events, such as footstrikes during basketball jump shots and running, have significant power in higher frequencies up to 50Hz [Edwards et al. 2010; Simons and Bradshaw 2016; Zhang et al. 2008], which may be attenuated when aggressively filtering motion capture data.

These high acceleration impact events play a substantial role in exciting soft tissue dynamics [James and Pai 2002; Park and Hodgins 2008; Wu et al. 2016b]. In the simplest analogue, soft tissue can be represented as an oscillatory second-order spring-damper system that is excited by an impulse to the base (skeleton). These second-order systems oscillate with an amplitude that scales with the impulse magnitude at a frequency that is characterized by the system's properties. Thus, to generate realistic soft tissue motion in dynamic human activities, it becomes necessary to accurately

capture both the true generalized accelerations of human motion and soft tissue properties.

Previous studies modeling soft tissue motion during dynamic activities have validated powerful data-driven techniques to relate internal skeletal motions estimated by motion capture with observed surface deformations [Javier et al. 2015; Park 2006; Park and Hodgins 2008]. However, these techniques inherently assume the internal skeleton trajectories from a motion capture system are accurate. Thus, inaccuracies in estimating impact accelerations remain a limitation for these data-driven reconstruction methods as well.

Accurately capturing impact accelerations is common practice in head injury biomechanics, where researchers utilize high rate IMU sensors sampling at up to 1000Hz [Kuo et al. 2018a; Siegmund et al. 2016; Wu et al. 2016b]. Characterizing head impacts typically seen in contact sports, researchers found that head impact kinematics have significant power in frequencies up to 200Hz [Wu et al. 2016a], well above effective bandwidths of typical motion capture systems after filtering. However, previous techniques for accurately measuring head impact generalized accelerations have been limited to the head due to sensor limitations (the ideal instrumented mouthguard form factor rigidly couples to the upper dentition), and a lack of integration with standard motion capture systems.

Despite these limitations, head impact research provides valuable insight into the requirements for measuring whole body impact accelerations. In this study, we present and experimentally implement a general method using high rate IMUs to correct whole body generalized velocities and accelerations around impact events measured with standard motion capture techniques. Our method is designed to make minimal changes to the generalized coordinates obtained from motion capture systems while simultaneously recovering impulse accelerations and associated near instantaneous changes in generalized velocity. To show the effectiveness of our method for animation purposes, we couple our corrected motions with a soft tissue rig to demonstrate minimal changes in gross motion while exciting substantial soft tissue dynamics. With our correction method, animators will have the capability of generating both lifelike gross human motion and realistic soft tissue motion during dynamic activities for creating ever more believable characters and animations. More generally, our method may be useful for predicting soft tissue dynamics and simulating impacts in biomechanics and other applications in clinical sciences.

2 THEORY

For our correction method, we make the assumption that body parameters ℓ such as mass, height, and body segment lengths are known (typically obtained from scanning or motion capture calibration). Furthermore, we assume that the location of high rate IMUs on the body \vec{r} is known. These locations can either be constant (rigidly attached to the skeleton) or a function of generalized coordinates \vec{q} (barycentric coordinate representation of skin surface locations).

2.1 Human Motion Modeling

From motion capture, we expect a representation of the measured human motion as a continuous, twice-differentiable, time-varying

signal of generalized coordinates $\vec{q}(t)$ that represent the configuration of the body. These generalized coordinates are typically body segment positions and orientations with respect to the laboratory inertial frame, or relative joint angles. From the generalized coordinates, we can identify the position and orientation of the i^{th} high rate IMU \vec{p}_i at time t as a function of the generalized coordinates \vec{q}_t , the body parameters ℓ , and the location of the IMU on the body \vec{r}_i . This is typically referred to as forward kinematics.

$$\vec{p}_i(t) = f(\vec{q}(t), \vec{r}_i, \ell) \quad (1)$$

Because high rate IMUs measure linear accelerations and angular velocities, we are interested in the derivatives of Equation 1 to obtain the accelerations \vec{a} and velocities \vec{v} predicted by the motion capture system at the high rate IMU locations.

$$\hat{v}_i(t) = \frac{d}{d\vec{q}} f(\vec{q}(t), \vec{r}_i, \ell) * \dot{\vec{q}}(t) = J(\vec{q}(t), \vec{r}_i, \ell) * \dot{\vec{q}}(t) \quad (2)$$

$$\hat{a}_i(t) = \dot{J}(\vec{q}(t), \vec{r}_i, \ell) * \dot{\vec{q}}(t) + J(\vec{q}(t), \vec{r}_i, \ell) * \ddot{\vec{q}}(t) \quad (3)$$

Where J is the Jacobian matrix and \dot{J} is its time derivative, which contains coriolis and centripetal terms. Differentiation can also be performed numerically as in [Abramowitz and Stegun 1965].

2.2 Correction Optimization

Now that we can compute the predicted accelerations and velocities at the high rate IMU locations using the motion capture generalized coordinates, we can correct the motion capture generalized coordinates in the time window $[t_i, t_f]$ during which an impact occurs. Common methods for identifying impacts and defining an impact window include thresholding on the measured linear acceleration. Once an impact window is defined, we superpose a correction function $c(t, \Phi_j)$ on a generalized coordinate $q_j(t)$. Each correction function acts in the impact window and is parameterized by Φ_j . For the continuous case, the first and second derivatives of the correction function should exist (C^2 continuous).

$$q_j(t)^* = q_j(t) + c(t, \Phi_j) \quad \forall t \in [t_i, t_f] \quad (4)$$

Using the corrected generalized coordinates, we can then define corrected accelerations $\hat{a}_i^*(t)$ and velocities $\hat{v}_i^*(t)$ at the high rate IMU locations.

$$\hat{v}_i^*(t) = J(\vec{q}^*(t), \vec{r}_i, \ell) * (\dot{\vec{q}}(t) + \begin{bmatrix} \dot{c}(t, \Phi_1) \\ \dot{c}(t, \Phi_2) \\ \vdots \\ \dot{c}(t, \Phi_n) \end{bmatrix}) \quad (5)$$

$$\hat{a}_i^*(t) = \dot{J}(\vec{q}^*(t), \vec{r}_i, \ell) * (\dot{\vec{q}}(t) + \begin{bmatrix} \dot{c}(t, \Phi_1) \\ \dot{c}(t, \Phi_2) \\ \vdots \\ \dot{c}(t, \Phi_n) \end{bmatrix}) + J(\vec{q}^*(t), \vec{r}_i, \ell) * (\ddot{\vec{q}}(t) + \begin{bmatrix} \ddot{c}(t, \Phi_1) \\ \ddot{c}(t, \Phi_2) \\ \vdots \\ \ddot{c}(t, \Phi_n) \end{bmatrix}) \quad (6)$$

To find the optimal correction, we solve for the correction function parameters Φ_j that minimize a weighted average of two cost functions (equation 7).

$$\Phi = \underset{\Phi}{\operatorname{argmin}} \alpha * \tau^2 * L_1(\Phi) + (1 - \alpha) * L_2(\Phi) \quad (7)$$

With τ as a time constant scaling factor. The first cost function L_1 is the square error between the predicted high rate IMU accelerations $\hat{a}^*(t)$ and velocities $\hat{v}^*(t)$, and the measured high rate IMU accelerations $\vec{a}(t)$ and velocities $\vec{v}(t)$. This cost function is designed to recover impact acceleration signal lost in motion capture filtering.

$$L_1(\Phi) = \sum_{t=t_i}^{t_f} \tau^2 * (\hat{a}^*(t) - \vec{a}(t))^T (\hat{a}^*(t) - \vec{a}(t)) + (\hat{v}^*(t) - \vec{v}(t))^T (\hat{v}^*(t) - \vec{v}(t)) \quad (8)$$

The second cost function L_2 is the maximum absolute value of the function $c(t, \Phi_j)$ (the infinity-norm) squared and is designed to minimize the correction on the original motion capture generalized coordinates.

$$L_2(\Phi) = \sum_{j=1}^n ||c(t, \Phi_j)||_\infty^2 \quad (9)$$

Conceptually, we can see how this correction procedure works by considering a sinusoid correction function parameterized with small amplitudes $a \ll 1$ at high frequencies $\omega \gg 1$ ($\Phi = (a, \omega)$).

$$c(t, a, \omega) = -a \sin(\omega t) \quad (10)$$

In this case, the correction function amplitude is small by definition, but the derivative amplitude is amplified.

$$\dot{c}(t, a, \omega) = -a\omega \cos(\omega t) \quad (11)$$

$$\ddot{c}(t, a, \omega) = a\omega^2 \sin(\omega t) \quad (12)$$

Returning to equation 6, we see that this results in an increase in acceleration estimate proportional to ω^2 .

3 METHODS

With the theoretical framework for impact correction laid out, we now demonstrate our method experimentally. In this section, we will describe our specific hardware, experimental procedures, and theoretical implementation to correct impacts in real world human motion capture measurements. We also describe our soft tissue

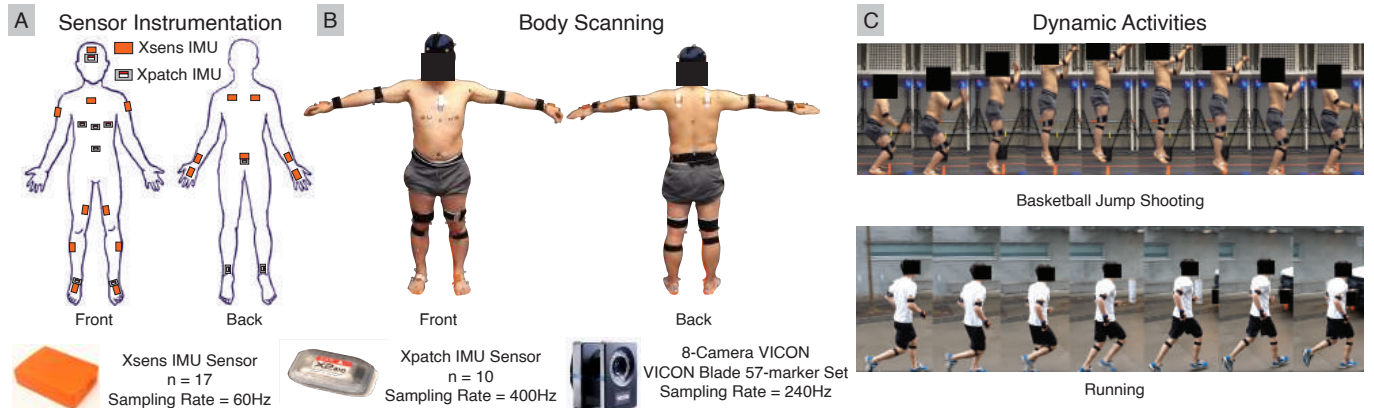


Fig. 2. Experimental Protocol for Implementing Impact Correction: (A) We equipped subjects with a Xsens Awinda suit (Xsens, Netherlands) as our motion capture system, which contains 17 sensors placed on the body. We further equipped subjects with a sparse sampling of 10 high rate Xpatch IMU sensors (X2 Biometrics, USA) on the torso and feet for impact correction. One subject also wore 57 optical markers arranged according to instructions provided in the VICON Blade software manual to track using a 10-camera VICON system. (B) We obtained a body scan of each subject to localize sensors with respect to the body and each other before having subjects perform (C) dynamic activities such as basketball jump shots and running.

simulation to visualize the effect of impact correction on creating realistic soft tissue animations in dynamic activities.

3.1 Experimental Protocol

To demonstrate our correction method, we collected real world human motion measurements using an IMU-based motion capture system (Awinda IMU suit, Xsens, Netherlands) [Roetenberg et al. 2009] and an optical marker-based motion capture system (VICON Blade, VICON Motion Systems, UK). Note that *any* motion capture method could be used; our implementation did not use the IMUs that are a part of the Awinda system for motion correction. For motion correction, we augmented the system with a sparse set of high rate IMUs (Xpatch, X2 Biometrics, USA) [Kuo et al. 2018a; Wu et al. 2016b]. Five subjects were recruited for this study and provided written informed consent (University of British Columbia Research Ethics Board, protocol H18-03342). All procedures adhered to the standards of the Declaration of Helsinki.

The Xsens Awinda suit included 18 IMUs, 17 of which were required for capturing full body motion (Figure 2). Awinda IMUs were placed according to manufacturer instructions, though individual units on the torso and feet were adhered directly to the skin using hypoallergenic double-sided tape. For full body capture, the Awinda suit is only capable of sampling at 60Hz, and each Awinda IMU unit has a linear acceleration range of $\pm 16g$ and angular velocity range of $\pm 2000deg/s$. The suit was calibrated using the standard N-pose and walk protocol as specified by Xsens, achieving at least a manufacturer-defined good calibration.

The VICON system was only implemented in one subject as the limited capture volume of the VICON system prevented us from capturing dynamic human activities outdoors. We used a 57 full body marker set as defined in the VICON Blade manual (defined in the Range of Motion section) tracked with 10 VICON cameras (8 MX cameras, 2 Vantage cameras, Figure 2). We calibrated the cameras using the wand wave procedure as outlined in the VICON

Blade manual, and also performed several range of motion protocols with the subject as outlined in the VICON Blade manual. We set the VICON capture rate to 240Hz, which was the highest frame rate that we could achieve without sacrificing camera resolution.

Ten high rate Xpatch IMUs were adhered to the skin using hypoallergenic double-sided tape at the top of each foot; the back of each foot above the heel; on the lumbar region of the back; on the stomach next to the belly button; on each pectoralis major muscle; on the center of the sternum; and on the forehead (Figure 2). Xpatch sensors were programmed to capture data at 400Hz with a linear acceleration range of $\pm 100g$ and angular velocity range of $\pm 2000deg/s$. Due to Xpatch IMU memory constraints, only seven minutes of continuous data were recorded at a time.

Prior to sensor placement, Xpatch sensors and the extra Awinda IMU were first time synchronized with each other. This was accomplished by placing sensors on a rigid object and applying a common angular motion to all sensors at once. For the subject instrumented with the optical markers, we used a trigger signal from the VICON system to simultaneously start and end recordings of the VICON optical tracker and Awinda IMU suit, and then time synced the Xpatch sensors to the extra Awinda IMU as before. Once sensors were placed, we used a laser body scanner (Vitus 3D Body Scanner, Human Solutions, Germany) to capture the 3 dimensional placement of sensors on the body. Subjects were then instructed to perform dynamic sports activities such as basketball jump shots and running to generate dynamic motions for correction. Note, the subject who was equipped with the VICON optical markers only performed basketball jump shots due to the limited capture volume of the camera system. Once data were collected, sensors were time synchronized once more to account for potential clock drift.

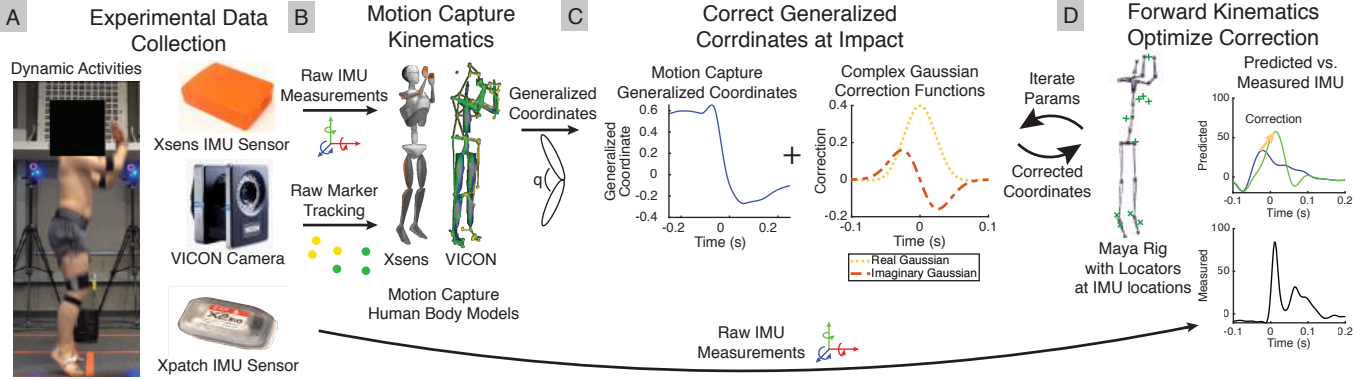


Fig. 3. Implemented Correction Algorithm for Experimental Data: (A) We measured human motion in dynamic activities experimentally using the Xsens Awinda motion capture suit and high rate Xpatch IMUs. One subject was additionally instrumented with the VICON Blade optical marker tracking system. (B) Xsens Awinda data were automatically processed in MVN studio 2019 using a human body model to solve for generalized coordinates (joint angles and root position and orientation). Similarly, optical marker tracking was post processed in VICON Blade first by labeling markers according to the 57 full body marker set, and then fitting a human body model to solve for generalized coordinates (joint angles and root position and orientation). (C) Generalized coordinates from both Xsens and VICON were exported to Maya to drive a human skeletal rig, where we applied correction functions around the impact windows. (D) We computed the predicted IMU measurements based on forward kinematics using the Maya rig and locators placed at high rate Xpatch IMU locations, and compared predicted IMU kinematics against the actual measurements. This was used to optimize correction function parameters.

3.2 Data Processing

Awinda suit motion capture data were streamed directly to a laptop (Microsoft Surface Core i5-7300U @ 2.60GHz, 8.0GB RAM, Windows 10) running MVN Studio 2019 (Figure 3A). We used MVN HD postprocessing with a multi-level setting to obtain human motion generalized coordinates (Figure 3B) prior to exporting a .fbx motion capture file to Maya (Autodesk, USA). We chose Maya as it is a common animation program that also provides convenient tools such as the forward kinematics functions in equations 1-3 and a python scripting environment for implementing the correction algorithm.

The VICON marker tracking data were streamed directly to a desktop (Xeon E5-2630 @2.4GHz, 128.0GB RAM, Windows 10) running VICON Blade (Figure 3A). We first ran an automatic marker labeling procedure before manually corrected markers that were mislabeled or unlabeled due to marker drop-out or cross-talk. We then ran the VICON Blade Solver to fit a human skeleton to the marker data (Figure 3B) prior to exporting a .fbx motion capture file to Maya. Note, during the solve process, we did not explicitly use any of the VICON Blade filters.

In Maya, we fit a standard humanIK rig with a total of 66 degrees of freedom to the motion capture data (instructions provided by Xsens). The time series for each generalized coordinate was represented by a continuous spline with keypoints at each time point for which the Awinda suit recorded a measurement. A similar humanIK rig was fit to the VICON data.

Xpatch data were downloaded to the same laptop and manually post-processed in Matlab 2018b (Mathworks, USA). We filtered linear acceleration and angular velocity signals using a fourth-order, zero-phase butterworth lowpass filter with a 200Hz (Nyquist limit) and 110Hz (manufacturer-specified bandwidth) cutoff respectively. Xpatch data were then oriented to match the Xsens root frame in

the N-pose configuration (x-axis anterior-posterior, y-axis superior-inferior, z-axis left-right).

Sensor orientations with respect to the body were identified in the body scan image by identifying the corners of each sensor and fitting a right-handed frame. The orientation of the pelvis root frame was determined by identifying landmarks on the body scan. The line between the Anterior Superior Iliac Spine (ASIS) of each iliac crest represented the left-right axis, while the line between the top of the head to the midpoint between the ASIS of each iliac crest represented the superior-inferior axis. The anterior-posterior axis was found by taking the cross product of the superior-inferior and left-right axes. Finally to guarantee an orthogonal coordinate system, the superior-inferior axis was corrected by taking the cross product of the left-right axis and the anterior-posterior axis.

3.3 Impact Correction

To obtain the forward kinematic estimates of high rate IMU positions, velocities, and accelerations using the Maya skeletal rig, we first rigidly fixed locators to the Maya rig at the location of each high rate IMU (\vec{r}_i). To assist with placement of the locators, we imported and scaled subject body scans into Maya and visually placed locators to match scanned Xpatch IMU sensor locations.

From this, we could query the position and orientation of the high rate IMU locators with respect to the ground-fixed frame at the Xpatch sample times, and numerically differentiate positions with a 4th order stencil to obtain velocities and accelerations [Abramowitz and Stegun 1965] (Figure 3D). For correction, we chose to superpose either the real or imaginary part of the complex Gaussian function onto the generalized coordinates (Equation 13, Figure 3C).

$$c(t, s_j, \sigma_j, \mu_j) = \frac{s_j}{\sqrt{2\pi}} \exp(\sqrt{-1} \frac{(t - \mu_j)}{\sigma_j}) \exp\left(\frac{(t - \mu_j)^2}{2\sigma_j^2}\right) \quad (13)$$

The complex Gaussian function is convenient as it is twice differentiable and can be parameterized with an amplitude scaling factor s_j , a standard deviation σ_j , and a mean time μ_j ($\Phi_j = (s_j, \sigma_j, \mu_j)$). Furthermore, the real part of the complex Gaussian function is monophasic and resembles an impulse, whereas the imaginary part of the complex Gaussian function is biphasic and resembles an acceleration-deceleration pulse.

To identify impact events, we used a thresholding technique to find vertical (superior-inferior) linear accelerations in the pelvis high rate IMU exceeding $25m/s^2$. A positive vertical acceleration threshold of $25m/s^2$ was chosen to capture both jumping and running footstrike impacts while also discarding non-impact events. Impact windows were defined as extending 100ms before threshold crossing and 150ms after threshold crossing ($t_f - t_i = 250ms$). This was adapted from standard techniques for identifying head impacts in previous literature [Kuo et al. 2018b; Wu et al. 2018].

For our implementation, we corrected the vertical linear position of the pelvis root using the real part of the complex Gaussian correction function, and the flexion angle of each ankle using the imaginary part of the complex Gaussian correction function, as these were primarily where our high rate Xpatch sensors were located. This allowed us to only optimize nine parameters to correct each impact. We chose a weighting term of $\alpha = 0.5$ to equally weight generalized acceleration error (Equation 8) and change in generalized coordinates (Equation 9). We empirically selected a time scaling factor of $\tau = 0.55s$ to scale the various terms in the cost function. Optimization was performed using scipy minimize (scipy version 0.19.1) with the Nelder-Mead method, implemented in Maya’s scripting environment.

3.4 Soft Tissue Simulation

Finally, we used the uncorrected and corrected motion capture to drive an animation of soft tissue dynamics. We used a generic human male soft tissue rig with a “sliding thick skin” soft tissue model recently proposed by [Pai et al. 2018], in which the skeletal motion is kinematically coupled to moving Dirichlet boundary conditions on the soft tissue. Please see that paper for details of the soft tissue model. We emphasize that our method is not dependent on any particular soft tissue model so long as the tissue motion is driven by a skeletal rig.

For comparison, we also collected 1000fps high frame rate video (Sony RX100, Sony Corporation, Japan) of a subject performing basketball jumps on a hard surface and on a cushion. The hard surface mimicked the surface on which subjects performed basketball jumps in our experimental trials, while the cushion was meant to dampen the basketball jump impact to mimic the effect of motion capture filtering. To better observe tissue deformations, we drew features on the subject’s stomach and tracked those features using Matlab’s vision toolbox tools 200ms around each basketball jump impact. We then computed the displacement of each marker with respect to the subjects’ hips to estimate the tissue deformation. Subject pelvis accelerations were measured using an Xpatch high rate sensor for comparison against experimental results.

4 RESULTS

Over the five subjects recruited, we observed 185 impacts during basketball jump shots and 1266 impacts during running using our thresholding method. Example thresholding of the pelvis vertical linear acceleration is shown in Figure 4 for basketball jump shots and running in one subject. While our thresholding method reliably

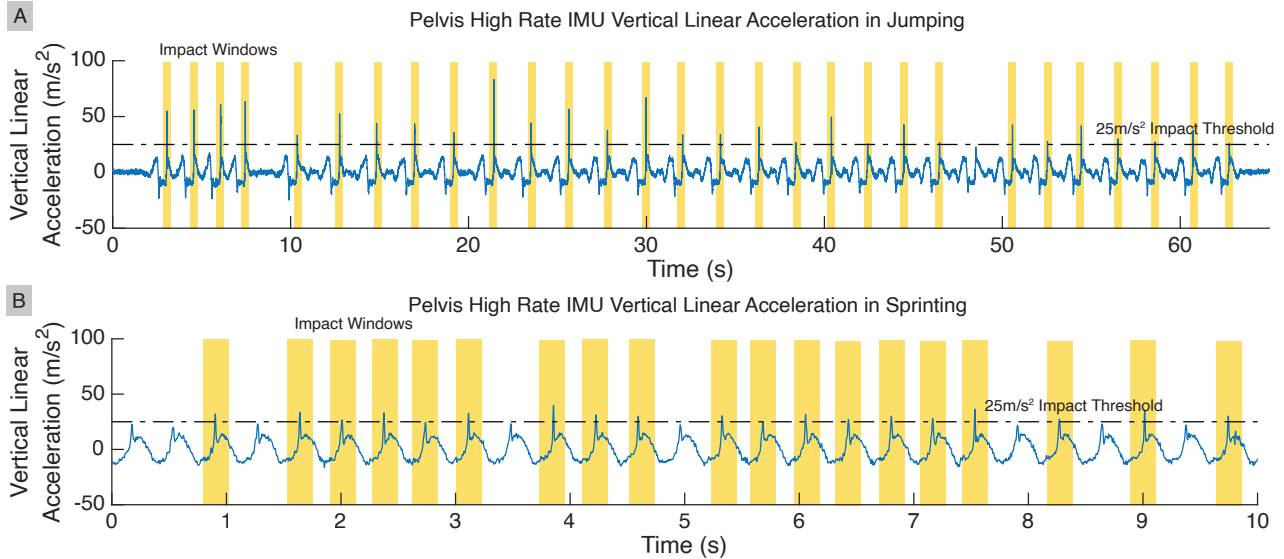


Fig. 4. Impact Threshold and Windowing: Example pelvis high rate Xpatch IMU vertical linear acceleration traces for a single subject during (A) basketball jump shots and (B) running. Impacts were identified when vertical linear acceleration crossed the $25m/s^2$ threshold and windows were defined from 100ms pre-threshold to 150ms post-threshold. While this threshold could capture jumping impacts well, some running impacts were missed.

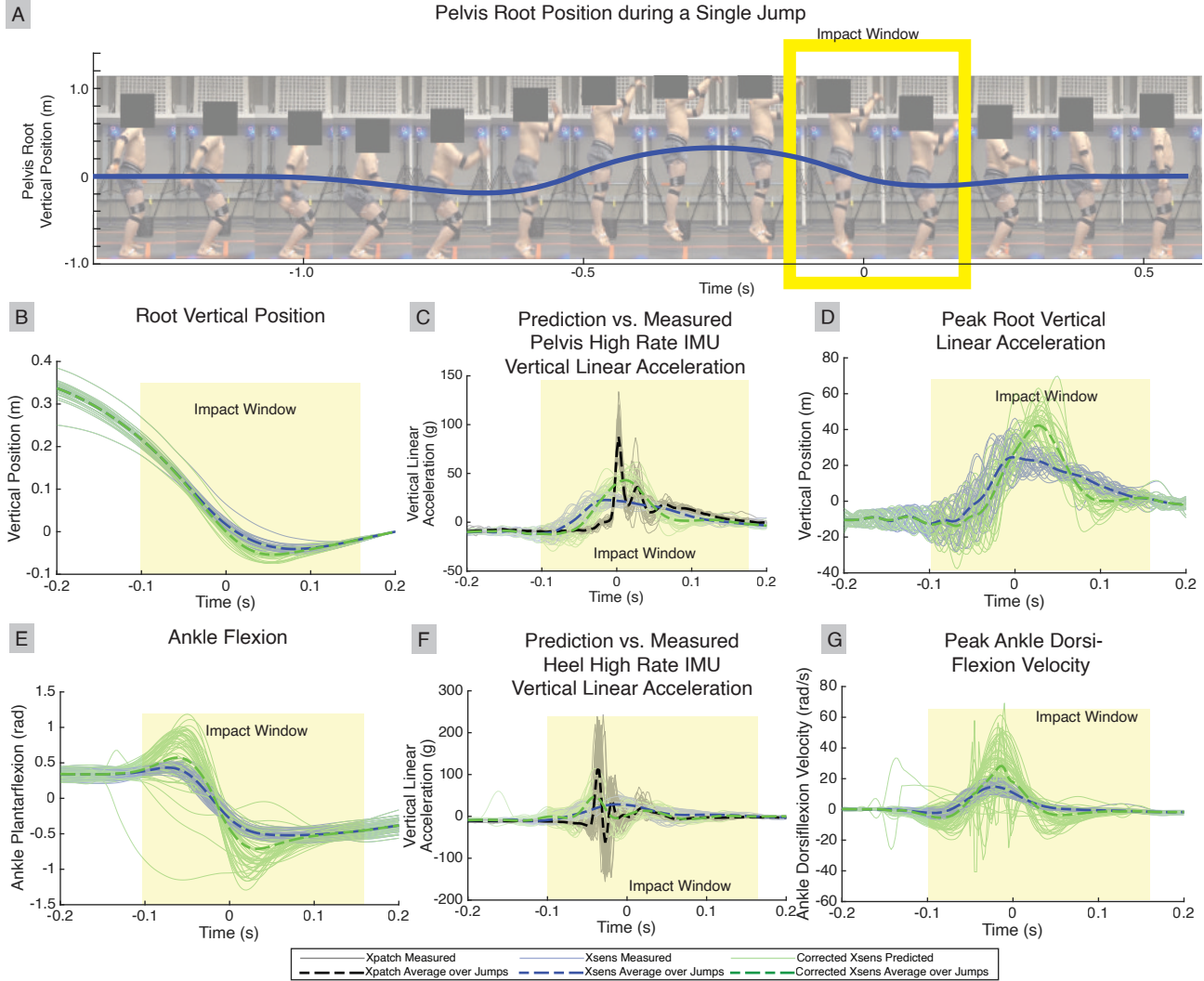


Fig. 5. Impact Corrections during Basketball Jumping: (A) Typical basketball jump shots took 2.0 seconds from crouching to flight to landing. The impact windowing procedure focused on the 250ms around the impact which occurred at landing. This figure details impact traces for a single subject with $n = 30$ jumps. Our algorithm made corrections of $2.5 \pm 0.9\text{cm}$ and $0.35 \pm 0.27\text{rad}$ to the (B) pelvis vertical position and (E) ankle flexion angle (both left and right ankles) respectively. Corrections were optimized to match vertical linear accelerations in Xpatch IMU sensors, such as (C) the pelvis IMU and (F) the heel IMUs. These corrections yielded changes in (D) root vertical linear acceleration of $22.6 \pm 9.2\text{m/s}^2$ and (G) ankle dorsiflexion velocity of $20.0 \pm 14.3\text{rad/s}$.

identified basketball jump shot impacts, some running footstrokes were below the threshold.

Figures 5 and 6 show time traces for one subject wearing the Xsens Awinda IMU suit with 30 individual basketball jump shot impacts and 273 individual running footstrokes respectively. For both activities, we observed small corrections in generalized coordinates that resulted in larger corrections in the generalized accelerations and velocities.

Over all impacts in all subjects, we also found similar small corrections in generalized coordinates with larger corrections in resulting accelerations and velocities. On average for basketball jump shot

impacts, our correction algorithm made generalized coordinate corrections of $1.9 \pm 1.3\text{cm}$ and $0.18 \pm 0.19\text{rad}$ to the pelvis root vertical position and ankle flexion angle respectively. Despite small generalized coordinate changes, pelvis root vertical linear accelerations were increased $23.6 \pm 19.2\text{m/s}^2$ (84.6%). Ankle dorsiflexion velocities were corrected with an increase of $12.1\text{rad/s} \pm 16.1\text{rad/s}$ (91.1%).

For running footstrokes, pelvis root vertical position saw corrections of $0.44 \pm 0.59\text{cm}$ resulting in pelvis root vertical linear acceleration increases of $17.3 \pm 16.8\text{m/s}^2$ (110%). Ankle flexion angle saw corrections of $0.11 \pm 0.09\text{rad}$ resulting in ankle plantarflexion velocity increases of $23.5 \pm 22.7\text{rad/s}$ (237%).

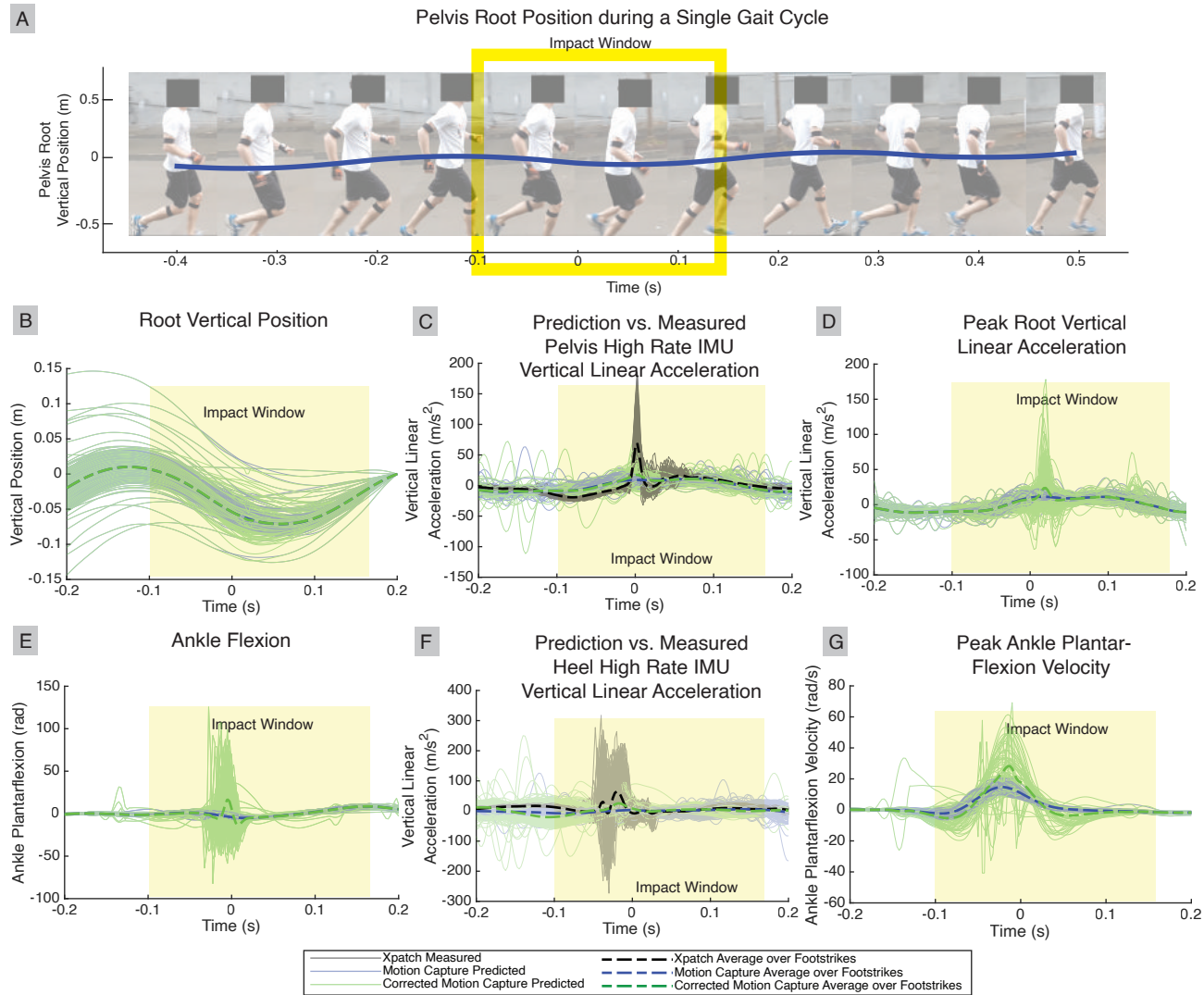


Fig. 6. Impact Corrections during Running: (A) Typical running gait cycle from one footstrike to the same footstrike. The impact windowing procedure focused on the 250ms around each footstrike. Most subjects ran at a cadence of 3-4 footstrikes per second. This figure details footstrike traces for a single subject with $n = 273$ footstrikes. Our algorithm made corrections of $0.54 \pm 0.64\text{cm}$ and $0.15 \pm 0.10\text{rad}$ to the (B) pelvis vertical position and (E) ankle flexion angle (both left and right ankles) respectively. Corrections were optimized to match vertical linear accelerations in Xpatch IMU sensors, such as (C) the pelvis IMU and (F) the heel IMUs. These corrections resulted in changes in (D) root vertical linear acceleration of $20.9 \pm 23.5\text{m/s}^2$ and (F) ankle plantarflexion velocity of $46.3 \pm 24.9\text{rad/s}$. Note, corrections were made in ankle plantarflexion for running and ankle dorsiflexion for jumping (opposite signs).

Of note, while the ankle flexion angle saw a smaller change in running than in jumping (0.11rad vs. 0.17rad respectively), the velocity change was greater in running than in jumping (23.5rad/s vs. 12.1rad/s respectively). This is because both the magnitude and standard deviation parameters of the Gaussian correction function were smaller for running, resulting in a smaller yet shorter duration generalized coordinate correction, which was amplified when differentiated. These differences were not statistically significant; however this highlights how the parameterization of the Gaussian correction function can produce different correction behaviors.

In Figure 7, we show results for the subject who wore both the Xsens Awinda IMU suit and VICON optical motion tracker system in basketball jumps. The original generalized coordinates from both the Xsens Awinda IMU suit and the VICON optical marker trakcer were similar, differing by $1.2 \pm 0.8\text{cm}$ and $0.05 \pm 0.04\text{rad}$ over the basketball jump shows in pelvis vertical position and ankle plantarflexion angle respectively. Because the generalized coordinates were similar, our algorithm made similar corrections to both, though the resulting increase in linear accelerations predicted at the high rate Xpatch locations were higher in the Xsens corrected kinematics compared with the VICON corrected kinematics (Figure 7).

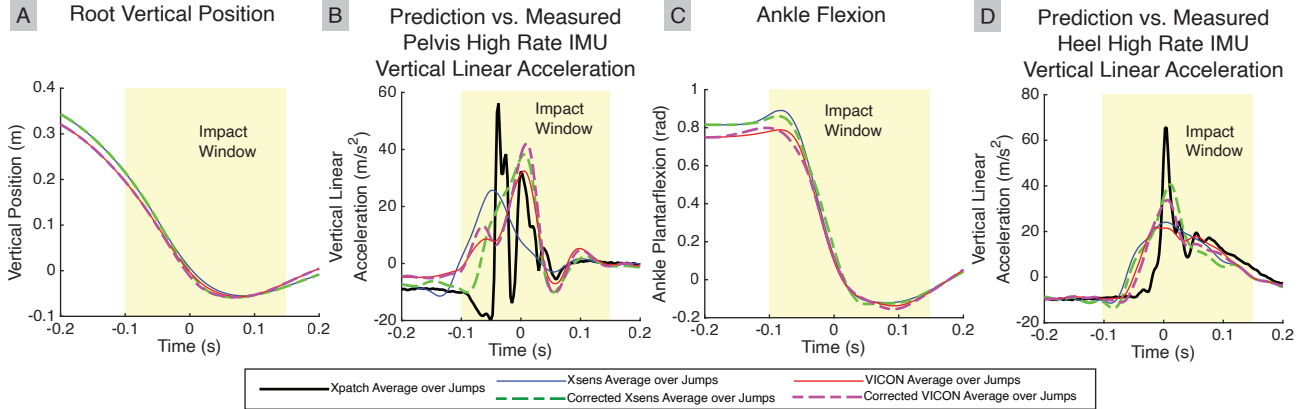


Fig. 7. Comparing Correction Algorithm on VICON and Xsens Motion Capture: In this figure, we show how our algorithm made similar corrections to generalized coordinates obtained from the subject who wore both the Xsens Awinda IMU suit and the VICON optical motion tracker system in $n = 30$ basketball jumps. The generalized coordinates obtained from both the Xsens and VICON systems were similar, differing by less than $2.0 \pm 1.2\text{cm}$ and $0.43 \pm 0.06\text{rad}$ on average in (A) pelvis vertical position and (C) ankle plantarflexion angle (both feet) respectively. Because of the similarity in their generalized coordinates, our algorithm made similar corrections in the Xsens and VICON generalized coordinates to best match the high rate Xpatch data. Corrections of $0.5 \pm 0.7\text{cm}$ and $0.4 \pm 1.0\text{cm}$ in (A) pelvis vertical position in Xsens and VICON respectively yielded increases of $17.4 \pm 22.7\text{m/s}^2$ and $10.5 \pm 19.2\text{m/s}^2$ in the predicted (B) pelvis Xpatch vertical linear acceleration in Xsens and VICON respectively. Corrections of $0.09 \pm 0.20\text{rad}$ and $0.08 \pm 0.24\text{rad}$ in (A) ankle plantarflexion angle in Xsens and VICON respectively yielded increases of $18.0 \pm 16.4\text{m/s}^2$ and $11.8 \pm 15.9\text{m/s}^2$ in the predicted (B) heel Xpatch vertical linear acceleration in Xsens and VICON respectively.

Figure 8 shows the effect of the corrected impact accelerations on the resulting skin motion animation for a single basketball jump shot and sequence of running footstrikes. While there was no perceptible change in the gross whole body motion, we found greater oscillations of the skin tissue following correction. Skin tissue oscillation amplitudes increased by 143.4% at the stomach for the example basketball jump shot shown in Figure 8A (increase of 2.2cm), while skin tissue oscillation amplitudes increased by 11.2% at the stomach for the example running sequence (containing several footstrikes) shown in Figure 8C (increase of 0.3cm). Figure 8 also shows soft tissue displacement results for the subject that was tracked with 1000fps high speed video. Skin tissue displacement at the stomach increased by 1.8cm from jumping on a cushion (representing motion capture filtering) to jumping on a hard surface (representing the corrected ground-truth).

5 DISCUSSION

We present a general method utilizing high rate inertial measurement unit (IMU) sensors to correct filtered motion capture generalized accelerations around impacts in dynamic activities. We further implemented this method utilizing a sparse set of Xpatch IMUs sampling at 400Hz to correct dynamic human motion from an Xsens Awinda IMU motion capture suit and for one subject, from a VICON optical marker tracking system, in basketball jump shots and running. Corrected accelerations had minimal effect on the motion capture estimated generalized coordinates, but excited substantial soft tissue motion due to the recovery of the impact impulse.

While we demonstrated a specific implementation based on popular motion capture systems and Maya animation software, our general method can be adapted to other hardware, software, and motions of interest. Motion capture can be performed using other

techniques such as single camera systems [Cao et al. 2017; Ionescu et al. 2014; Kanazawa et al. 2018; Wei et al. 2016] so long as human motions are represented using generalized coordinate time traces. Furthermore, implementation of forward kinematics to predict high rate IMU accelerations can be performed in other animation or analysis software such as Blender and OpenSim. Finally, animators can place high rate IMUs on other body segments, such as the arms, to recover impact accelerations to the whole body.

We demonstrate briefly the generalizability of our implementation by performing the correction algorithm on one subject wearing both the Xsens Awinda IMU suit and VICON optical marker trackers performing basketball jump shots. We showed that both systems generated similar generalized coordinates through their normal processing pipelines (in MVN Studio and VICON Blade respectively), differing by $2.0 \pm 1.2\text{cm}$ and $0.43 \pm 0.06\text{rad}$ in pelvis vertical position and ankle plantarflexion angles respectively over the basketball jump shots. While our correction algorithm made substantial corrections to both the Xsens and VICON kinematics (increase of over 10m/s^2 in predicted Xpatch accelerations), we note that there were greater increases in predicted Xpatch accelerations in the corrected Xsens kinematics compared to the corrected VICON kinematics. This could be because the VICON data were collected at a higher sampling rate (240Hz vs. 60Hz) and thus had less attenuation of the impact kinematics.

With our specific implementation of the correction method, we recovered impact accelerations from basketball jump shots and running activities measured experimentally. In both activities, small corrections to the generalized coordinates (pelvis root vertical position and ankle flexion angles) resulted in large increases in pelvis root vertical linear accelerations and ankle plantar- or dorsiflexion velocities, though the amount of correction varied between subjects

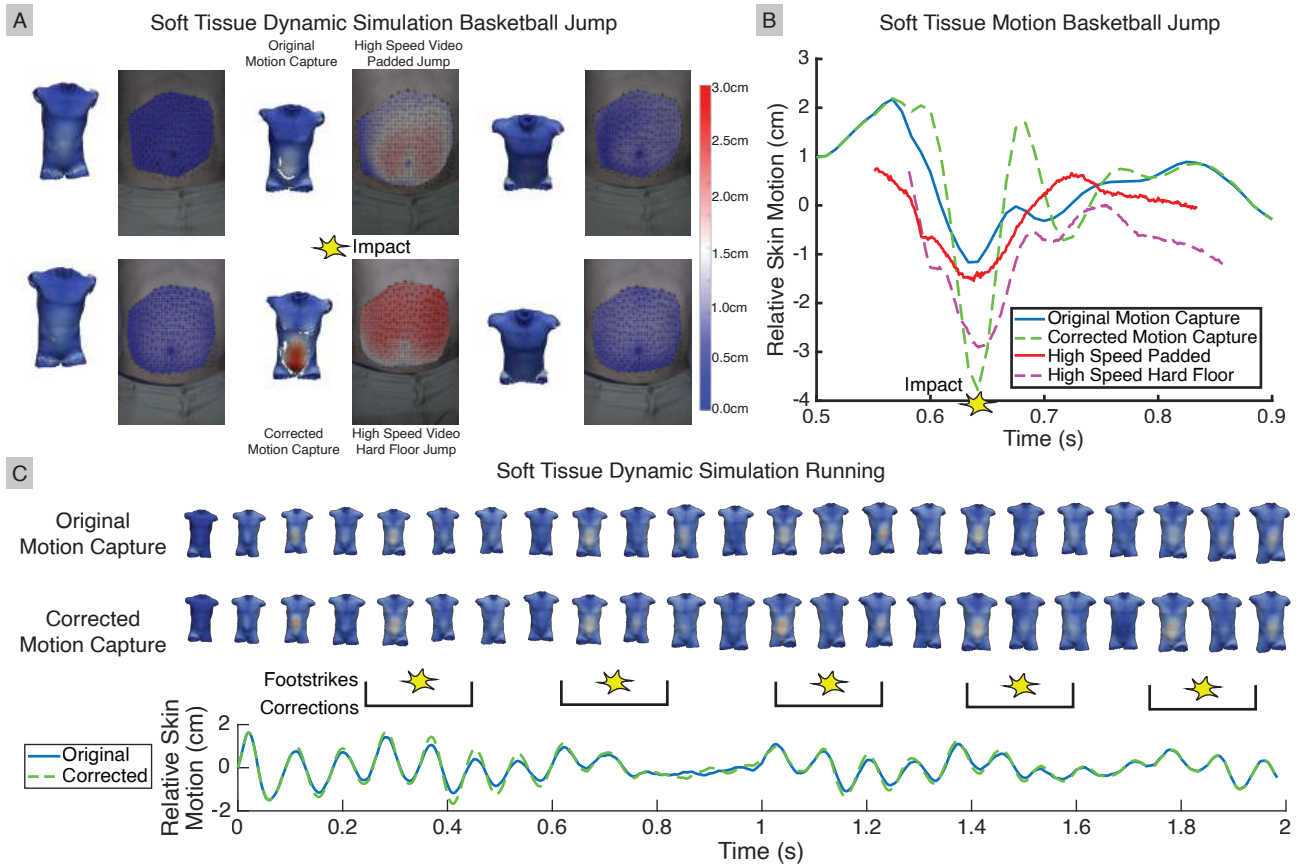


Fig. 8. Effect of Corrections on Soft Tissue Dynamics: Our algorithm made relatively small corrections to the gross generalized coordinates, but yielded relatively large corrections in accelerations and velocities. These accelerations and velocities are responsible for exciting soft tissue dynamics. (A) To show the effect of these corrections, we simulated both original and corrected motions with a soft tissue dynamics rig and observed the difference in soft tissue motion. (B) Corrected jumping motion exhibited increased soft tissue motion of 2.2cm for this impact, which had a correction of 3.5cm to the pelvis root vertical position and 25.6m/s^2 to the pelvis root vertical linear acceleration. We compare this to high speed video of tissue deformations for one subject who jumped on a soft cushion (representing motion capture filtering) and a hard surface (representing corrected ground-truth accelerations). Similar increases of 1.8cm in soft tissue deformations are observed in the high speed video, where the subject had pelvis accelerations of 50m/s^2 and 65m/s^2 on the cushion and hard surface respectively (measured using an Xpatch high rate sensor). (C) Corrected running motion exhibited smaller changes to soft tissue motion (0.5cm), but due to the increased frequency of footstrike impacts in running, there was almost a continuous difference in soft tissue dynamics following correction.

(as evidenced by a small ankle dorsiflexion velocity correction in the subject shown in Figure 5 compared to the average over all subjects). The large increases in the derivatives was likely due to the short time durations of the correction Gaussian functions (100ms in jumping and 10ms in running), which were amplified when differentiated. Specifically in running, the short duration Gaussian corrections recovered a dual acceleration peak that is characteristic of heel strike impacts during running (Figure 6).

While successful in recovering accelerations and velocities with minor changes to the generalized coordinates, there are several nuances that could inform future implementation of our algorithm. First, we discuss our choice of a monophasic correction function for pelvis root vertical position and a biphasic correction function for ankle flexion angle. The second derivative (generalized acceleration correction) of the monophasic correction function resembles

an impulse and is perhaps best suited for recovering dynamics of impacts, such as strikes to the body. The second derivative of the biphasic correction function resembles a fast acceleration followed immediately by a deceleration and is perhaps best suited for recovering joint buckling such as in the ankles, knees, and hips. We chose the complex Gaussian as our correction function because it was easily parameterized (with three parameters representing a time offset, an amplitude, and a duration) and yielded both a monophasic and biphasic behavior. However, the Gaussian correction function typically did not fully correct for attenuated acceleration signals. Other correction functions with more tunable parameters might be required to fully recapture attenuated accelerations, but will also require more computation time due to the additional parameters to optimize.

Second, corrections are activity dependent, as observed by the larger corrections in basketball jump shots. This could be because impact impulses during jumping have higher accelerations and shorter durations than in running. Motion capture filters more heavily attenuate shorter duration impulses, requiring larger corrections. From this observation, it is possible that our correction method is not necessary for relatively mild activities such as walking where impacts have lower accelerations and longer durations.

Finally, we observed an increased plantarflexion ankle velocity in basketball jump shots and an increased dorsiflexion ankle velocity in running over our subjects. This is likely due to how the foot strikes the ground in these activities, with the toes touching first in basketball jump shots and the heel touching first in running. Thus, our correction method increased ankle velocity in the original direction of motion for both activities.

5.1 Limitations

While we demonstrate the capability of our method for correcting impact accelerations to generate realistic skin motion dynamics, there are some limitations to this study. First, there currently is no method to get the true generalized accelerations of body segments, as both IMU sensors and video markers are placed on soft tissue that decouple and oscillate over the skeleton during impacts. While we use the high rate IMU sensors to recover impact acceleration lost to filtering in motion capture, the accelerations and velocities measured by the high rate IMU sensors are not necessarily representative of the true skeleton accelerations. Recent work has demonstrated that it is possible to estimate skeleton accelerations using a Kalman filter and a network of IMU sensors adhered to a single body segment, but this method requires multiple sensors to obtain estimates for a single body segment [Kuo et al. 2018a].

Second, our correction method currently does not run in real-time. Specifically, the optimization procedure takes on the order of minutes per 250ms impact window. While this prevents real-time use, we note that our correction method runs with similar speed or substantially faster than Xsens HD motion correction, animation rendering, and finite element soft tissue simulations. Thus, our correction method should not substantially prolong animation pipelines when used in conjunction with other post-processing steps.

Finally, our skin motion model has not been validated in a dynamic regime. Of note, our soft tissue model currently lacks viscous terms that are responsible for decaying soft tissue oscillations post impact. As a result, we observed highly underdamped soft tissue dynamics in our simulation when compared to the high speed video of a human subject in Figure 8. Despite this, the soft tissue motion magnitude predicted by our simulations compared favorably to live human soft tissue deformations captured using 1000fps high speed video. Future work could tune soft tissue material models in dynamic events by matching skin accelerations to the high rate IMU measurements or high speed video.

5.2 Conclusion

In conclusion, we have developed a method for recovering impact accelerations from filtered motion capture data using a sparse set of high rate IMUs. This method can be used to generate more lifelike

soft tissue motions during dynamic activities commonly seen in sports while retaining the accurate gross motion estimates obtained from validated motion capture systems. Furthermore, as demonstrated with our specific implementation which utilized only wearable IMUs, we highlight the capability of simulating soft tissue dynamics without the need for complicated video-based methods. Future directions for this work could include using different types of sensors to correct impact signals (such as force or pressure transducers) and using corrected signals to excite clothing dynamics.

ACKNOWLEDGMENTS

We would like to acknowledge our funding sources: NSERC Idea-to-Innovation grant, Vital Mechanics Research Inc., and Killam Postdoctoral Research Fellowship. Additional support was provided by ICICS, Canada Foundation for Innovation, NSERC Discovery grants, and the Canada Research Chairs Program. We would also like to acknowledge Pearson Wyder-Hodge for assistance with VICON data collection and Gunter P. Siegmund for providing Xpatch sensors.

REFERENCES

- Milton Abramowitz and Irene Stegun. 1965. *Handbook of mathematical functions: with formulas, graphs, and mathematical tables*. Number 55. Dover Publishing, Washington, D.C.
- Nathaniel A. Bates, Kevin R. Ford, Gregory D. Myer, and Timothy E. Hewett. 2013. Impact differences in ground reaction force and center of mass between the first and second landing phases of a drop vertical jump and their implications for injury risk assessment. *Journal of Biomechanics* 46, 7 (2013), 1237–1241. <https://doi.org/10.1016/j.jbiomech.2013.02.024>
- Zhe Cao, Tomas Simon, Shih-En Wei, and Yaser Sheikh. 2017. Realtime multi-person 2d pose estimation using part affinity fields. In *Proceedings of the IEEE Conference on Computer Vision and Pattern Recognition*, 7291–7299. <https://doi.org/10.12693/APhysPolA.106.709> arXiv:1611.08050
- Pietro Cerveri, Antonio Pedotti, and Giancarlo Ferrigno. 2003. Robust recovery of human motion from video using Kalman filters and virtual humans. *Human movement science* 22, 3 (2003), 377–404. [https://doi.org/10.1016/S0167-9457\(03\)00004-6](https://doi.org/10.1016/S0167-9457(03)00004-6)
- Pietro Cerveri, Antonio Pedotti, and Giancarlo Ferrigno. 2005. Kinematical models to reduce the effect of skin artifacts on marker-based human motion estimation. *Journal of Biomechanics* 38, 11 (2005), 2228–2236. <https://doi.org/10.1016/j.jbiomech.2004.09.032>
- Ross A. Clark, Yong-hao Pua, Karine Fortin, Callan Ritchie, Kate E. Webster, Linda Denney, and Adam L. Bryant. 2012. Gait & Posture Validity of the Microsoft Kinect for assessment of postural control. *Gait & Posture* 36, 3 (2012), 372–377. <https://doi.org/10.1016/j.gaitpost.2012.03.033>
- William B. Edwards, David Taylor, Thomas J. Rudolfi, Jason C. Gillette, and Timothy R. Derrick. 2010. Clinical Biomechanics Effects of running speed on a probabilistic stress fracture model. *Clinical Biomechanics* 25, 4 (2010), 372–377. <https://doi.org/10.1016/j.clinbiomech.2010.01.001>
- Kevin R. Ford, Gregory D. Myer, and Timothy E. Hewett. 2000. Valgus Knee Motion during Landing in High School Female and Male Basketball Players. *Medicine & Science in Sports & Exercise* 35, 10 (2000), 1745–1750. <https://doi.org/10.1249/01.MSS.0000089346.85744.D9>
- Giannis Giakas and Vasilios Baltzopoulos. 1997. A Comparison of Automatic Filtering Techniques Applied to Biomechanical Walking Data. *Journal of Biomechanics* 30, 8 (1997), 847–850.
- Michael Gleicher. 1999. Animation From Observation : Motion Capture and Motion Editing. *ACM SIGGRAPH Computer Graphics* 33, 4 (1999), 51–54.
- Samuel R. Hamner, Ajay Seth, and Scott L. Delp. 2010. Muscle contributions to propulsion and support during running. *Journal of Biomechanics* 43, 14 (2010), 2709–2716. <https://doi.org/10.1016/j.jbiomech.2010.06.025>
- Catalin Ionescu, Dragos Papava, Vlad Olaru, and Cristian Sminchisescu. 2014. Human3. 6m: Large scale datasets and predictive methods for 3d human sensing in natural environments. *IEEE transactions on pattern analysis and machine intelligence* 36, 7 (2014), 1325–1339.
- Doug L. James and Dinesh K. Pai. 2002. DyRT: dynamic response textures for real time deformation simulation with graphics hardware. *ACM Transactions on Graphics (TOG)* 21, 3 (2002), 582–585. <https://doi.org/10.2514/1.A32984>
- Gerard Pons-moll Javier, Romero Naureen, and Mahmood Michael. 2015. Dyna : A Model of Dynamic Human Shape in Motion. *ACM Transactions on Graphics (TOG)* 34, 4 (2015).

- Angjoo Kanazawa, Michael J. Black, David W. Jacobs, and Jitendra Malik. 2018. End-to-end Recovery of Human Shape and Pose. In *Proceedings of the IEEE Conference on Computer Vision and Pattern Recognition*. 7122–7131. <https://doi.org/10.1109/CVPR.2018.00744> arXiv:1712.06584
- Calvin Kuo, Jake Sganga, Michael Fanton, and David B. Camarillo. 2018a. Head impact kinematics estimation with network of inertial measurement units. *Journal of Biomechanical Engineering* In Revisions (2018).
- Calvin Kuo, Lyndia C. Wu, Jesus Loza, Daniel Senif, Scott Anderson, and David B. Camarillo. 2018b. Comparison of video-based and sensor-based head impact exposure. *PLoS ONE* 13, 6 (2018), e0199238. <https://doi.org/10.1101/235432>
- Daniel L. Miranda, Paul D. Fadale, Michael J. Hulstyn, Robert M. Shalvoy, Jason T. Machan, and Braden C. Fleming. 2013a. Knee biomechanics during a jump-cut maneuver: effects of gender & ACL surgery. *Medicine and science in sports and exercise* 45, 5 (2013), 942–951. <https://doi.org/10.1097/BRSM.0b013e31828ca5c7>.Motion
- Daniel L. Miranda, Michael J. Rainbow, Joseph J. Crisco, and Braden C. Fleming. 2013b. Kinematic differences between optical motion capture and biplanar videoradiography during a jump – cut maneuver. *Journal of Biomechanics* 46, 3 (2013), 567–573. <https://doi.org/10.1016/j.jbiomech.2012.09.023>
- Thomas B. Moeslund and Eriik Granum. 2001. A Survey of Computer Vision-Based Human Motion Capture. *Computer Vision and Image Understanding* 81, 3 (2001), 231–268. <https://doi.org/10.1006/cviu.2000.0897>
- Thomas B. Moeslund, Adrian Hilton, and Volker Kru. 2006. A survey of advances in vision-based human motion capture and analysis. *Computer Vision and Image Understanding* 104, 2-3 (2006), 90–126. <https://doi.org/10.1016/j.cviu.2006.08.002>
- Dinesh K. Pai, Austin Rothwell, Pearson Wyder-Hodge, Alistair Wick, Ye Fan, Egor Larionov, Darcy Harrison, Debanga Raj Neog, and Cole Shing. 2018. The Human Touch : Measuring Contact with Real Human Soft Tissues. *ACM Transactions on Graphics (TOG)* 37, 4 (2018).
- Sang Il Park. 2006. Capturing and Animating Skin Deformation in Human Motion. *ACM Transactions on Graphics (TOG)* 25, 3 (2006), 881–889.
- Sang Il Park and Jessica K. Hodgins. 2008. Data-driven Modeling of Skin and Muscle Deformation. *ACM Transactions on Graphics (TOG)* 27, 3 (2008). <https://doi.org/10.1145/1360612.1360695>
- Katherine Pullen and Christoph Bregler. 2002. Motion Capture Assisted Animation : Texturing and Synthesis. *ACM Transactions on Graphics (TOG)* 21, 3 (2002), 501–508.
- Raziel Riemer, Elizabeth T. Hsiao-weksler, and Xudong Zhang. 2008. Uncertainties in inverse dynamics solutions : A comprehensive analysis and an application to gait. *Gait & posture* 27, 4 (2008), 578–588. <https://doi.org/10.1016/j.gaitpost.2007.07.012>
- Daniel Roetenberg, Henk Luinge, and Per Slycke. 2009. Xsens MVN : Full 6DOF Human Motion Tracking Using Miniature Inertial Sensors. Technical Report January 2009. 1–7 pages. <https://doi.org/10.1.1.569.9604>
- Thomas Seel, Jörg Raisch, and Thomas Schauer. 2014. IMU-Based Joint Angle Measurement for Gait Analysis. *Sensors* 14, 4 (2014), 6891–6909. <https://doi.org/10.3390/s140406891>
- Gunter P. Siegmund, Kevin M. Guskiewicz, Stephen W. Marshall, Alyssa L. DeMarco, and Stephanie J. Bonin. 2016. Laboratory Validation of Two Wearable Sensor Systems for Measuring Head Impact Severity in Football Players. *Annals of Biomedical Engineering* 44, 4 (2016), 1257–1274. <https://doi.org/10.1007/s10439-015-1420-6>
- Chantal Simons and Elizabeth J. Bradshaw. 2016. Do accelerometers mounted on the back provide a good estimate of impact loads in jumping and landing tasks ? estimate of impact loads in jumping and landing tasks ? *Sports Biomechanics* 15, 1 (2016), 76–88. <https://doi.org/10.1080/14763141.2015.1123765>
- Daniel Vlasic, Rolf Adelsberger, Giovanni Vannucci, John Barnwell, Markus Gross, Wojciech Matusik, and Jovan Popovic. 2007. Practical Motion Capture in Everyday Surroundings. *ACM transactions on graphics (TOG)* 26, 3 (2007). <https://doi.org/10.1145/1239451.1239480>
- Shih-En Wei, Varun Ramakrishna, Takeo Kanada, and Yaser Sheikh. 2016. Pose Machines .: In *Proceedings of the IEEE Conference on Computer Vision and Pattern Recognition*. <https://doi.org/10.1109/CVPR.2016.511> arXiv:arXiv:1602.00134v4
- Christopher R. Winby, David G. Lloyd, Thor F. Besier, and T. Brett Kirk. 2009. Muscle and external load contribution to knee joint contact loads during normal gait. *Journal of Biomechanics* 42, 14 (2009), 2294–2300. <https://doi.org/10.1016/j.jbiomech.2009.06.019>
- Lyndia C. Wu, Calvin Kuo, Jesus Loza, Mehmet Kurt, Kaveh Laksari, Livia Z. Yanez, Daniel Senif, Scott C. Anderson, Logan E. Miller, Jillian E. Urban, Joel D. Stitzel, and David B. Camarillo. 2018. Detection of American Football Head Impacts Using Biomechanical Features and Support Vector Machine Classification. *Scientific Reports* 8, 1 (2018), 1–14. <https://doi.org/10.1038/s41598-017-17864-3>
- Lyndia C. Wu, Kaveh Laksari, Calvin Kuo, Jason F. Luck, Svein Kleiven, Cameron R. Bass, and David B. Camarillo. 2016a. Bandwidth and sample rate requirements for wearable head impact sensors. *Journal of Biomechanics* 39, 0 (2016), 2918–2924. <https://doi.org/10.1016/j.jbiomech.2016.07.004>
- Lyndia C. Wu, Vaibhav Nangia, Kevin Bui, Bradley Hammoor, Mehmet Kurt, Fidel Hernandez, Calvin Kuo, and David B. Camarillo. 2016b. In Vivo Evaluation of Wearable Head Impact Sensors. *Annals of Biomedical Engineering* 44, 4 (2016), 1234–1245. <https://doi.org/10.1007/s10439-015-1423-3> arXiv:1503.03948
- Songning Zhang, Timothy R. Derrick, William Evans, Yeon-joo Yu, Songning Zhang, Timothy R. Derrick, William Evans, and Yeon-joo Yu. 2008. Shock and impact reduction in moderate and strenuous landing activities. *Sports Biomechanics* 7, 2 (2008), 296–309. <https://doi.org/10.1080/14763140701841936>